

C-19 and Hot, Wide, Star Streams

RAYMOND G. CARLBERG,¹ RODRIGO IBATA,² NICOLAS F. MARTIN,² ELSE STARKENBURG,³ DAVID S. AGUADO,⁴
KHYATI MALHAN,⁵ KIM VENN,⁶ AND ZHEN YUAN (袁珍)⁷

¹*Department of Astronomy & Astrophysics, University of Toronto, Toronto, ON M5S 3H4, Canada*

²*Université de Strasbourg, CNRS, Observatoire astronomique de Strasbourg, UMR 7550, F-67000 Strasbourg, France*

³*Kapteyn Astronomical Institute, University of Groningen, Landleven 12, 9747 AD Groningen, The Netherlands*

⁴*Instituto de Astrofísica de Canarias, Vía Láctea, 38205 La Laguna, Tenerife, Spain*

⁵*DARK, Niels Bohr Institute, University of Copenhagen, Jagtvej 128, 2200 Copenhagen, Denmark*

⁶*Department of Physics and Astronomy, University of Victoria, Victoria, BC, V8W 3P2, Canada*

⁷*School of Astronomy and Space Science, Nanjing University, Key Laboratory of Modern Astronomy and Astrophysics (Nanjing University), Ministry of Education, Nanjing 210093, China*

ABSTRACT

The C-19 star stream has the abundance characteristics of an unusually metal poor globular cluster but kinematically is uncharacteristically hot and wide for a cluster stream, having a line of sight velocity dispersion of 6 km s^{-1} and a 1-sigma width of 240 pc. We show that the tidal dissolution of an old, lower mass, globular cluster in a CDM galactic halo naturally creates a hot, wide stream currently near orbital apocenter. More generally, simulations show that hot streams, which are all near their orbital apocenter, become thin, cool streams near pericenter. Furthermore, the wide streams from a population of dissolved clusters in the simulations have a mean galactocentric radial velocity dispersion of $7.8 \pm 1.0 \text{ km s}^{-1}$ in a CDM cosmology but only $4.1 \pm 1.6 \text{ km s}^{-1}$ in a WDM (5.5 keV) simulation. A detailed C-19 model in a simplified Milky Way halo potential with a CDM subhalo population provides a lower bound to stream heating, finding that the stream develops a line of sight velocity dispersion of $4.1 \pm 1.1 \text{ km s}^{-1}$, whereas WDM (5.5 keV) subhalos give $3.1 \pm 0.1 \text{ km s}^{-1}$. Known dwarf galaxies alone provide negligible heating. There are five other currently known streams wider than 200 pc that contain a globular cluster, all near their orbital apocenter.

1. INTRODUCTION

The C-19 stream of extremely low metallicity stars (Martin et al. 2022) was discovered (Ibata et al. 2021) in the Gaia data (Gaia Collaboration et al. 2016) using the STREAMFINDER algorithm (Malhan & Ibata 2018). High resolution spectroscopy (Martin et al. 2022; Yuan et al. 2022) of photometrically identified low metallicity stream candidates (Starkenbourg et al. 2017) established that C-19 has a metal abundance of $[\text{Fe}/\text{H}] = -3.4$ with a 95% confidence $[\text{Fe}/\text{H}]$ spread of less than 0.2 (Martin et al. 2022). Further investigation has found additional stream candidates giving a length of more than 50 degrees (Yuan et al. 2022; Viswanathan et al. 2024). The spread in stellar abundances is close to the detection limit and the abundance patterns are characteristic of globular cluster stars (Yuan et al. 2022). The abundances and extrapolated luminosity of approximately

$10^4 L_{\odot}$ led Martin et al. (2022) to argue that the progenitor was more likely to be a disrupted globular cluster than a disrupted dwarf galaxy, while considering that the 1-sigma width of 240 pc, and line of sight velocity dispersion of 6 km s^{-1} were more in keeping with a disrupted dwarf. A dynamical model of a disrupting dark matter dominated dwarf galaxy can account for the kinematic properties of the stream (Errani et al. 2022).

The question addressed here is under what conditions can a globular cluster progenitor be compatible with the C-19 kinematic data. Most of the known streams in the compilation Galstreams (Mateu 2023) are thinner than C-19 with typical FWHM of 100 pc or less. On the other hand, simulations of globular cluster streams in realistic cosmological conditions find that the dark matter subhalos present in the galactic halo cause the velocity dispersion of stream stars to increase with time (Carlberg & Agler 2023). The average velocity distribution of long, thin streams has a core with extended wings (Carlberg 2018; Malhan et al. 2019). The width of the

wings increases with the numbers of subhalos present in the galactic halo (Carlberg et al. 2024). The velocity at which stars join the stream determines the width of the low velocity core of a stream. Subsequent encounters with subhalos perturb stars into the extended wings of the velocity and width distribution. The growing dataset for the GD-1 stream provides tentative evidence for the existence of a core-wing velocity structure (Ibata et al. 2024; Valluri et al. 2024).

The C-19 stream is on a nearly polar, inner halo orbit, 8-24 kpc, where the density of subhalos is relatively high, creating the circumstances for significant subhalo heating. The stream is composed of extremely metal poor, $[\text{Fe}/\text{H}] \simeq -3.4$, hence likely very old, stars in an inner halo orbit such that the moderate mass progenitor cluster likely dissolved relatively early and the stream has been subject to subhalo heating for much of the lifetime of the Milky Way.

In §2 we measure the range of widths and velocity dispersions of the streams that form in both CDM and WDM cosmological simulations from low mass globular clusters. We then use the cosmological simulations to motivate an evolving potential model for the Milky Way in which model star clusters on the orbit of C-19 are integrated and their velocity dispersions are measured to compare to C-19 in §3. The results are discussed §4 to assess the accuracy of the model and its ability to constrain the subhalo content of the Milky Way. Other currently known wide streams from globular clusters are briefly discussed along with the likelihood that there are other wide streams yet to be discovered.

2. LOW MASS STAR CLUSTERS IN COSMOLOGICAL SIMULATIONS

The total stellar mass of C-19 is estimated to be in the range 3×10^3 to $10^4 M_\odot$ (Martin et al. 2022; Yuan et al. 2022; Ibata et al. 2024). There is no visible progenitor, as expected for an old star cluster with a half mass relaxation time of 1-2 Gyr orbiting in the Milky Way (Gnedin & Ostriker 1997; Binney & Tremaine 2008; Errani et al. 2022). The C-19 stream has an angular momentum of about $3100 \text{ kpc} \cdot \text{km s}^{-1}$, and is on a moderate eccentricity, $e \simeq 0.45$, nearly polar, orbit within 25 kpc of the galactic center (Martin et al. 2022).

Two cosmological Milky Way-like simulations are seeded with low mass progenitor star clusters in the mass range $5\text{-}20 \times 10^3 M_\odot$ in a CDM cosmology and a WDM(5.5 keV) cosmology. The cosmological simulations of streams in Carlberg et al. (2024) contained progenitor clusters more massive than $4 \times 10^4 M_\odot$, most of which survive to the present epoch. Other than the initial star cluster masses, the simulations here are iden-

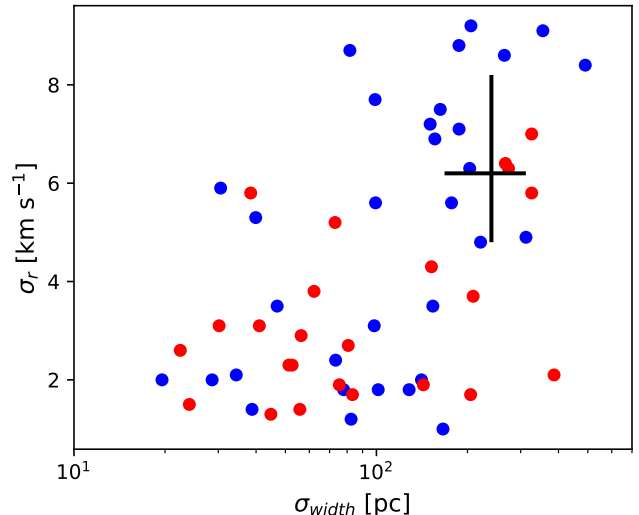


Figure 1. The stream radial velocity dispersion (galactocentric) vs stream width as measured perpendicular to the stream track for low mass cluster progenitors in cosmological simulations at the final time. CDM streams are blue points, WDM red. The error bar gives the C-19 values.

tical to those in Carlberg et al. (2024) and the same stream analysis procedures are used. We examine the simulation streams above a minimum angular momentum of $2000 \text{ kpc} \cdot \text{km s}^{-1}$, which excludes those that interact strongly with the disk. The streams are selected to be within 60 kpc of the galactic center. The velocity dispersion and width are measured for the central region of the stream above a surface density threshold of $20 M_\odot \text{ deg}^{-2}$ which approximately defines the readily detected part of streams. Figure 1 shows the stream radial velocity dispersion, after removing the mean, against stream width for the 32 CDM streams and 24 WDM streams longer than 10 degrees, the minimum angle for our search and analysis algorithm. The same plot for the more massive progenitor star clusters in Carlberg et al. (2024) shows a similar correlation of velocity dispersion and width for the streams which are about twice the length of the streams here but show less difference between CDM and WDM.

The distribution of stream stars projected onto the orbital plane varies from a narrow distribution at pericenter to extended “feathers” at apocenter, as illustrated in Figure 2 of Carlberg (2015). The orbital variation is a consequence of the galactic tidal field accelerating stars away from the cluster in a narrow radial band near pericenter, the subsequent orbital spreading of the unbound stars at apocenter, then regrouping at pericenter again, somewhat similar to the orbital dependence of velocities of an accretion remnant (Helmi & White 1999).

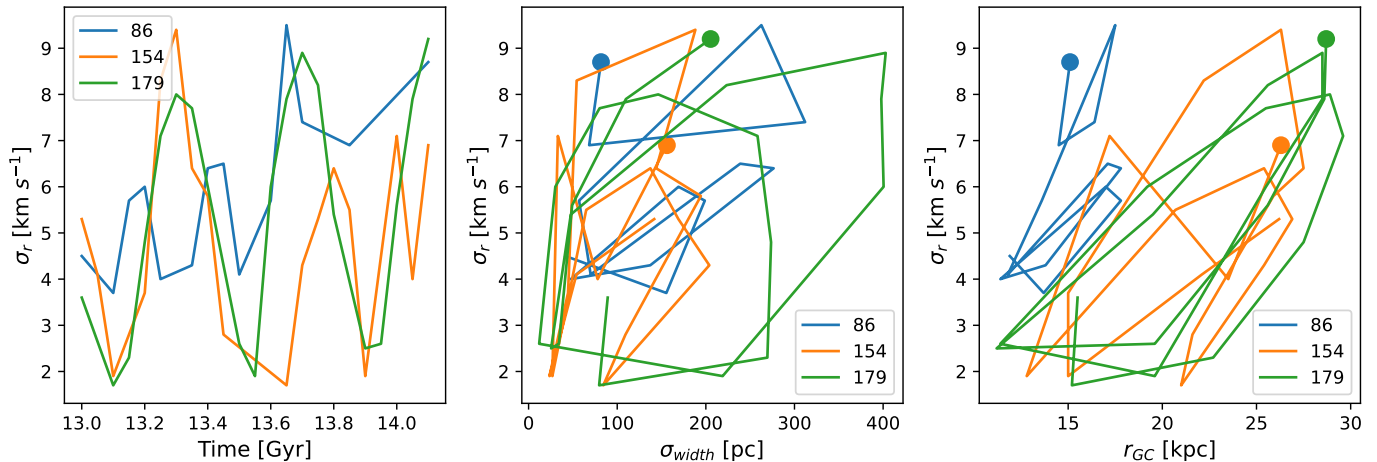


Figure 2. The orbital evolution of the stream radial velocity dispersion (left panel) with time for a few of the CDM streams selected to have a high velocity dispersion and $L \simeq 3000$ kpc- km s^{-1} at the final time, 14.1 Gyr. The final time is marked with a dot in the two rightmost panels. The middle panel shows tracks the evolution of velocity dispersion with width. The left panel shows the evolution of the radial velocity dispersion with galactocentric distance.

The variation of the radial velocity dispersion (galactocentric) and the average physical width with time for a few individual inner halo streams are shown in the left hand panel of Figure 2. The streams were selected to have angular momenta around 3000 kpc- km s^{-1} and velocity dispersion around 8 km s^{-1} , values comparable to those for C-19. The right hand panel shows the relation between the galactocentric σ_r and the galactic radius of the center of the streams. The streams from clusters 154 and 179 are on moderately eccentric orbits with σ_r varying from about 2-3 to 7-9 km s^{-1} as the stream orbits. Stream 86 is on a less eccentric orbit and shows smaller orbital variations in velocity dispersion and width. When near apocenter a stream’s structure is often visibly less well organized than at pericenter, with offshoots and bifurcations.

Figure 3 shows the radial velocity dispersion (left) and width (right) of all the CDM (top) and WDM (bottom) streams at the end of the simulation, over the 13-14.1 Gyr time interval, as a function of the fractional distance to apocenter. The 1.1 Gyr time range is just sufficient to capture the basic radial range of the most distant clusters in these samples, but not the full orbital complexity of the potentials. The point sizes are proportional to the orbital eccentricity. The figure shows that strong correlation of both σ_r and σ_{width} with the fractional distance to apocenter depends on orbital eccentricity, with a large scatter. The high eccentricity streams (larger point sizes) have the most extreme variation with apocenter distance and tend to have larger absolute velocity dispersions and widths.

The velocity distribution within a stream usually has an approximately Gaussian core with extended wings (Carlberg et al. 2024). The kurtosis of these velocity distributions is not very stable, so we characterize the velocity distribution using clipped variances of the distributions. The radial velocity dispersion is calculated along the length of the stream with 3-sigma clipping. The 6-sigma clipped velocity dispersion is typically a factor of two larger for streams with $\sigma_r \leq 3$ km s^{-1} as shown in Figure 4. As the streams pass near pericenter the velocity distribution narrows but leaves behind extended wings which are not present when the velocity distribution widens around apocenter.

Figure 5 shows that streams on high angular momentum orbits, those above 8000 kpc- km s^{-1} , have the velocity dispersion at which stars joined the streams, approximately 2 km s^{-1} . The medium size squares in Figure 5 identify the streams that are within 30 kpc of the galactic center. The mean of the radial velocity dispersion for streams inside 30 kpc are shown as the large squares, finding 7.8 ± 1.0 km s^{-1} for CDM and 4.1 ± 1.6 km s^{-1} for 5.5 keV WDM, where the error ranges are the spread of the population, not the error in the mean. Lower angular momentum streams orbit closer to the center of the galaxy where the subhalo density is higher than in the outskirts, and there are more subhalos in a CDM galactic halo than in a WDM version. Clearly, a stellar stream from a globular cluster progenitor can easily have a velocity dispersion of 6 km s^{-1} or more when the stream is near apocenter in a CDM galactic halo.

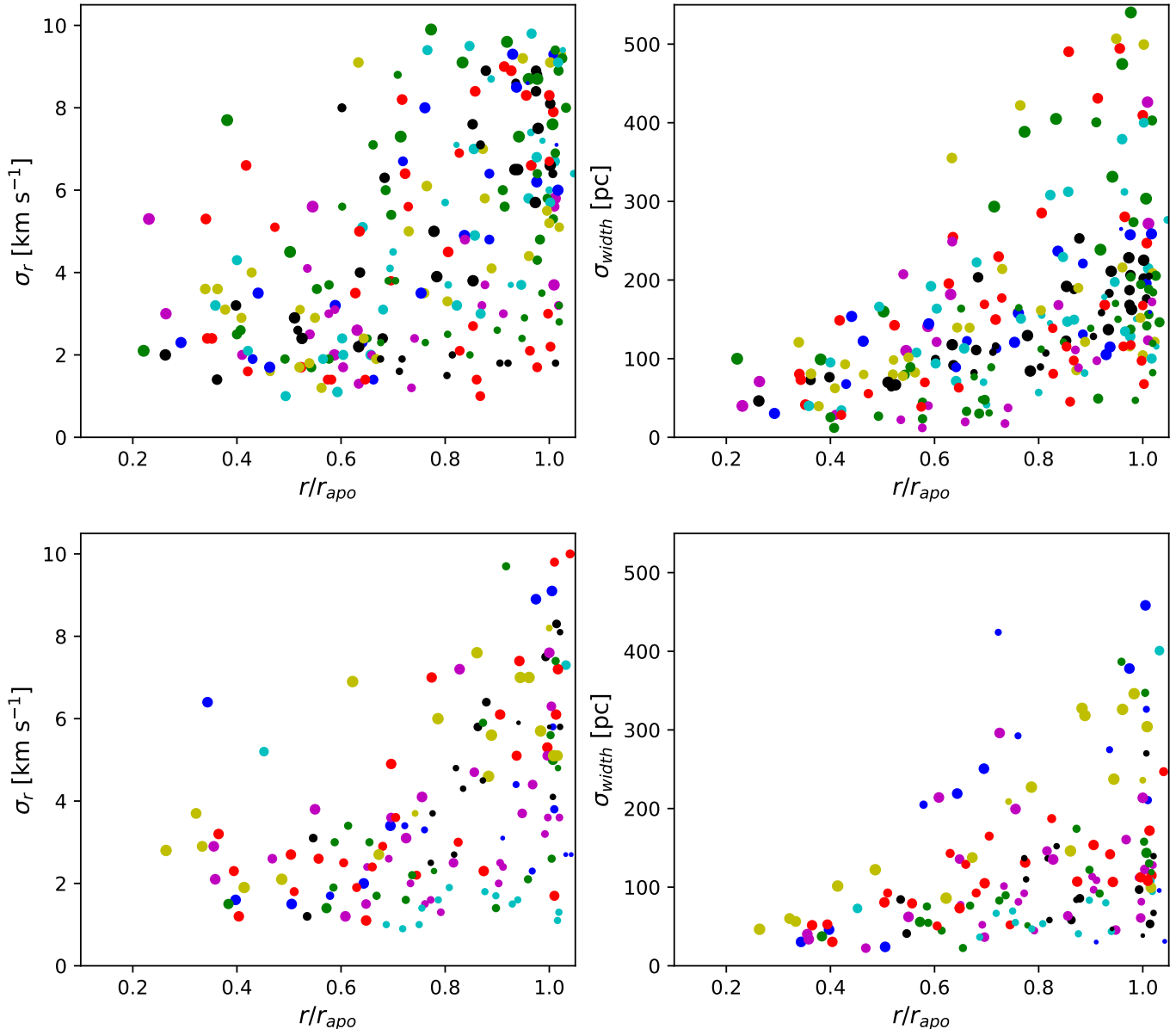


Figure 3. The stream radial velocity dispersions and widths with fractional distance to apocenter for the CDM (top) and WDM(5.5 keV) (bottom) streams. The point sizes are proportional to the orbital eccentricity. The colors change with time from 13 to 14.1 Gyr (the final time), in steps of 0.1 Gyr with a cycle of 7 colors.

Figure 6 shows two streams in the CDM simulation with a final time velocity dispersion above 6 km s^{-1} that orbit within 30 kpc. The particle plots usefully reveal the entire distribution of the dispersed cluster stars, but only the 20-30 degree segments at a galactic Y coordinate of approximately 20 kpc have sufficiently high sky density to be readily visible. The orbital history of these two clusters is shown in Figure 7. Cluster 154, shown in red, accretes onto the main halo in the first few Gyr of the simulation. Cluster 179, shown in green, is accreted around 7 Gyr, about halfway through the simulation.

Dynamical friction in the aspherical halo (Binney 1977) draws the subhalo containing the cluster into the plane of the galaxy and reduces the orbital angular momentum of the cluster.

3. MODELING THE C-19 STREAM

The globular cluster streams in the cosmological simulations have radial velocity dispersions that range from about 2 to 9 km s^{-1} , with the highest velocity dispersion at orbital apocenter. The highest density part of C-19 is just past orbital apocenter (Martin et al. 2022;

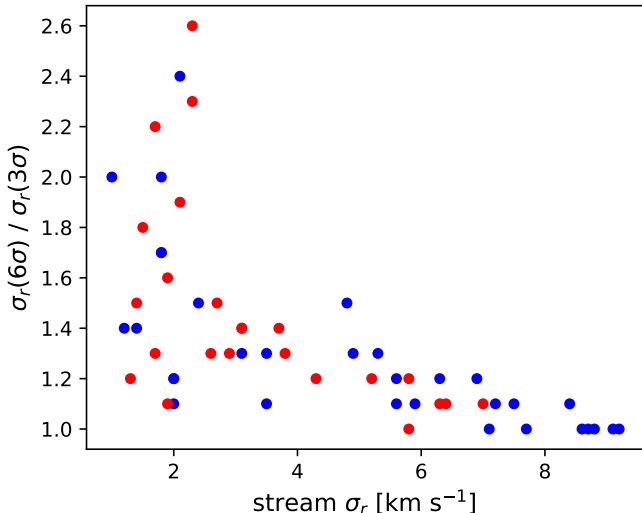


Figure 4. The ratio of the 6-sigma clipped radial velocity dispersion to the 3-sigma value vs the stream velocity dispersion. The 6-to-3 ratio is a measure of the size of the wings of the velocity distribution function. CDM streams are blue, WDM, red.

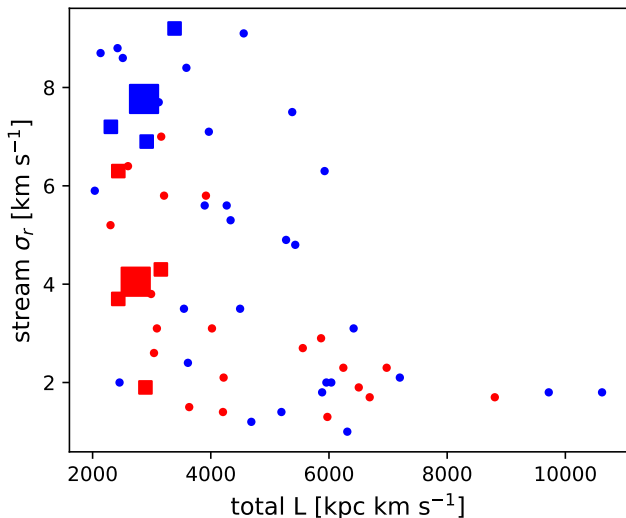


Figure 5. The mean galactocentric σ_r along the part of the stream above the density threshold with the (dissolved) progenitor angular momentum. All orbital phases are plotted. The CDM simulation streams are marked with blue and the WDM(5.5 keV) with red. The streams inside 30 kpc, with widths greater than 100 pc and angular momentum between 2000 and 4000 kpc-km s⁻¹ are shown as squares with the averages shown with the large squares.

Viswanathan et al. 2024) and is similar to the high velocity streams in the simulations. Detailed modeling of a star cluster on the C-19 orbit is useful to understand the conditions under which a wide, hot stream develops. In particular the subhalo heating of a stream depends on the number of subhalos present in the primary halo and the length of time that the stream has been orbiting after tidal removal from of its natal subhalo.

Our C-1 stream model is a simplification of the cosmological simulation to follow a single star cluster in a pre-computed version of the galactic potential. The model star cluster has a mass of $1 \times 10^4 M_\odot$, composed of $1 M_\odot$ star particles using the same star cluster simulation as in the full cosmological model. The initial half-mass radius is set to approximately 4 pc for the models reported here. The star particles have a softening of 1 pc and are integrated with the Gadget4 code (Springel et al. 2021). Two body interactions are included with small random velocities calculated from the relaxation time (Spitzer 1987; Binney & Tremaine 2008) added to star particles within the virial radius, about 5 pc, every 5 Myr (Carberg & Agler 2023). The tidal acceleration increases with distance from the cluster, pumping the stars into more distant orbits until they are swept away from the cluster (Meiron et al. 2021). The cluster-centric orbits become increasingly complex with distance (Fukushige & Heggie 2000). The cluster-centric radial coordinates of a sample of star particles are shown in Figure 8.

The potential in which the star cluster orbits is drawn from the cosmological simulation. The primary mass component is a static, triaxial NFW potential, with mass, $9.2 \times 10^{11} M_\odot$, virial radius 200 kpc, scale of 14.4 kpc, and density triaxiality from the AHF halo finder (Gill et al. 2004; Knollmann & Knebe 2009) measurements at the final moment the simulation. The potential triaxiality is set to $b/a=0.97$, $c/a=0.83$ using Equation 2.72a of Binney & Tremaine (2008). A Miyamoto-Nagai galactic bulge-disk (Miyamoto & Nagai 1975) grows within the halo using the model of Carberg et al. (2024). Although not important for the inner halo streams considered here, the LMC is included as a $1.8 \times 10^{11} M_\odot$ (Garavito-Camargo et al. 2019) Hernquist sphere (Hernquist 1990), which means that the barycenter of the system is offset from the center of the primary halo. The framework could include a more detailed buildup of the primary halo and include a rotating galactic bar both of which would provide some additional stream heating. The current sparse C-19 data does not require more than the basic model. The positions and velocities of the population of subhalos above $10^6 M_\odot$ as found in one of the full cosmological simulations at the chosen starting time is integrated in the

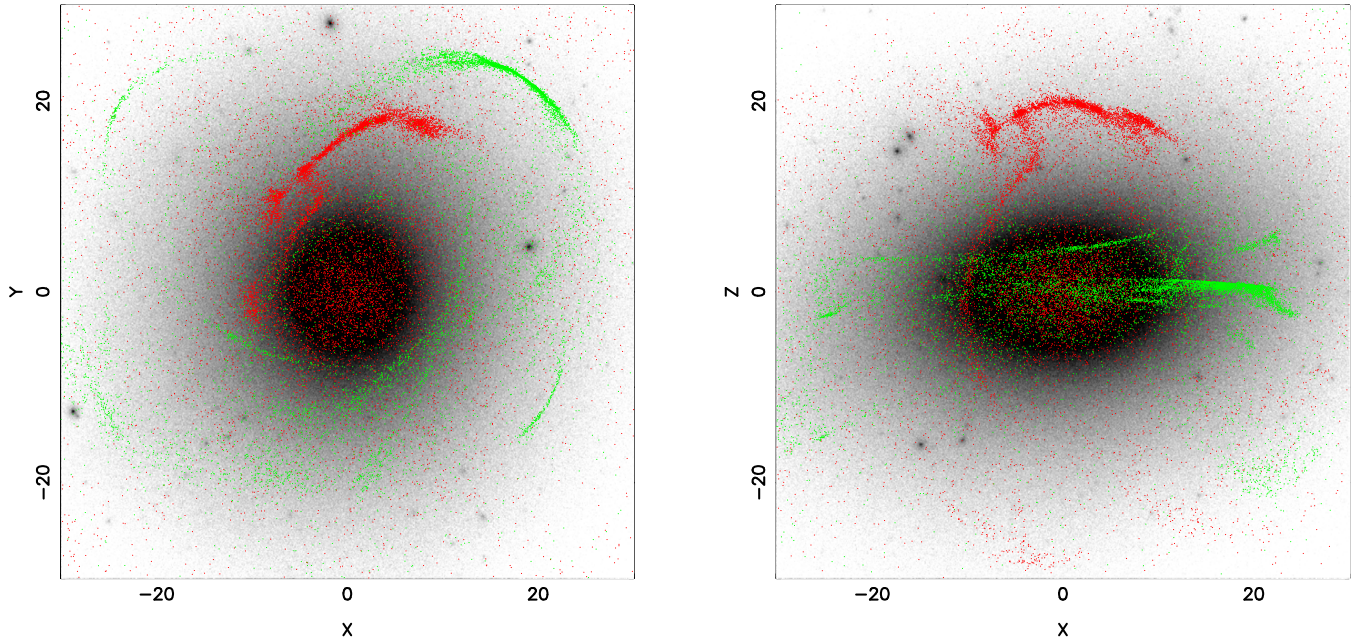


Figure 6. XY and XZ projections of two low angular momentum streams with radial velocity dispersion of 6.9 (red) and 9.2 km s^{-1} (green) that develop from two dissolved stars clusters with initial masses of 1.6 and $1.3 \times 10^4 M_{\odot}$ in the CDM simulation. The red stream is nearly polar whereas the green stream orbits near the galactic plane. Movies of the entire simulation and individually of these two streams are at [CDM Low Mass Clusters](#).

combined Milky Way dark halo, disk and LMC potential. The subhalos do not interact with each other. The subhalos' masses decrease in time with an exponential decay in time, with a timescale of 5.5 Gyr, measured from the subhalo numbers with time in the simulations. The decrease in subhalo mass with time means that the subhalo $N(> M)$ relation within the main halo declines approximately as measured in the fully dynamical cosmological simulations. Subhalos over the mass range $10^6 M_{\odot}$ to $3 \times 10^8 M_{\odot}$ are included. Lower mass halos have little dynamical effect on the stream and higher mass subhalos are expected to contain visible dwarf galaxies. All subhalos are modeled as Hernquist spheres with a scale radius equal to r_{max} from AHF. As the subhalos lose mass the radii are adjusted as $M^{1/3}$ to keep the characteristic density of each subhalo constant. In addition to the subhalos the 55 dwarf galaxies with kinematics (McConnachie 2012) are included. The dwarf galaxy dark halos are assigned maximal masses, $M = 5 \times 10^8 (L/L_{\odot})^{0.65} M_{\odot}$, which roughly match the high mass end of the subhalo mass distribution function. The dwarf galaxy halo radii are set to $a = 1.0 (M/10^8 M_{\odot})^{0.23} \text{ kpc}$, on the basis of the fit to the r_{max} mass relation of the subhalos in the simulations. All the subhalo orbits are precomputed and define spline

coefficients for the positions of the masses which the star cluster calculation uses as an external potential.

Figure 9 shows the model subhalo population in the inner halo along with the stream at a cosmological time of 13.1 Gyr, 1Gyr before the present time. For a CDM cosmology about 8200 subhalos are followed and 2800 for a WDM (5.5 keV) cosmology, both within the virial radius of 200 kpc. Most of the subhalos orbit well outside the region where C-19 orbits, but they are included for completeness. The dwarf galaxies are shown in green in Figure 9 although interactions are rare and usually do not influence inner halo streams (Bonaca et al. 2019). The XY projection of the stream is shown in grayscale at time 1 Gyr before present when stream particles are still passing through orbital apocenter. Subhalos that are within 2 scale radii of the stream are in blue and the stream particles within that radius are red. The interacting subhalo near the center of the image has a current mass of $2.2 \times 10^7 M_{\odot}$ and induces a velocity change of about 0.5 km s^{-1} in the nearest stream particles. The interactions that dominate the stream velocity variations are largely from more massive halos in the first 5-6 Gyr of the simulation, once the tidal tails have acquired appreciable length but before the subhalo interactions diminish as their masses decline.

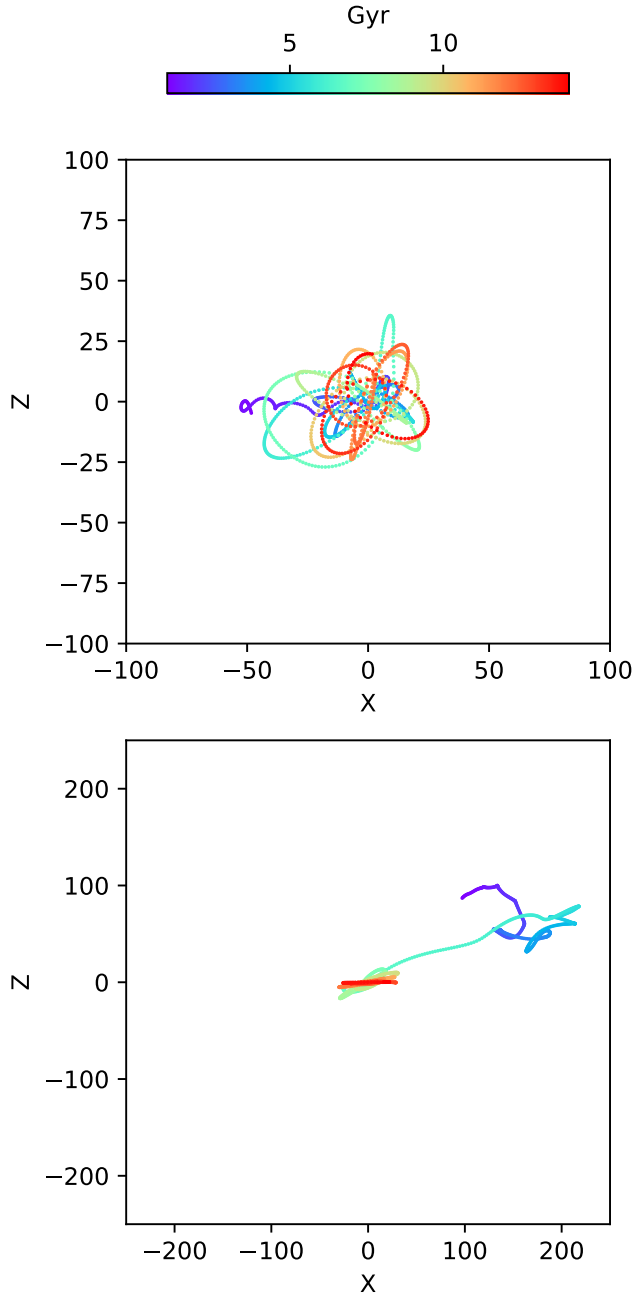


Figure 7. The orbits of the two clusters in Figure 6 relative to the center of the primary halo. Note that the scale is larger in the lower panels. The coordinates are with respect to the center of the dominant halo. The colors indicate the time within the simulation, from a 1 Gyr start (violet) to the 14.1 Gyr end time (red).

The evolving potential model presented here does a reasonable job capturing the interactions of subhalos with the stream but misses the larger scale interactions that scatter the older, more distant ends of the stream over the halo as shown in Figure 6 for the cosmologi-

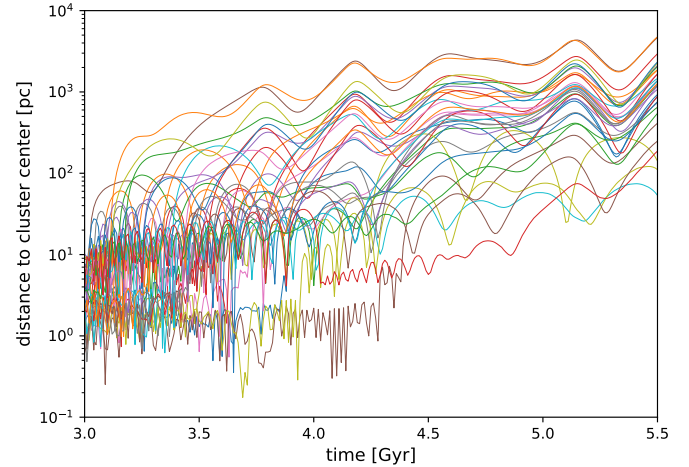


Figure 8. The distance from the star cluster center of star particles with time. The heating algorithm adds a random velocity, initially about 0.6 km s^{-1} , every 0.005 Gyr to the star particles between 3 to 4 pc. Tidal pumping raises particles over several orbits to the zero binding energy surface near 100 kpc after which they drift out to join the stream.

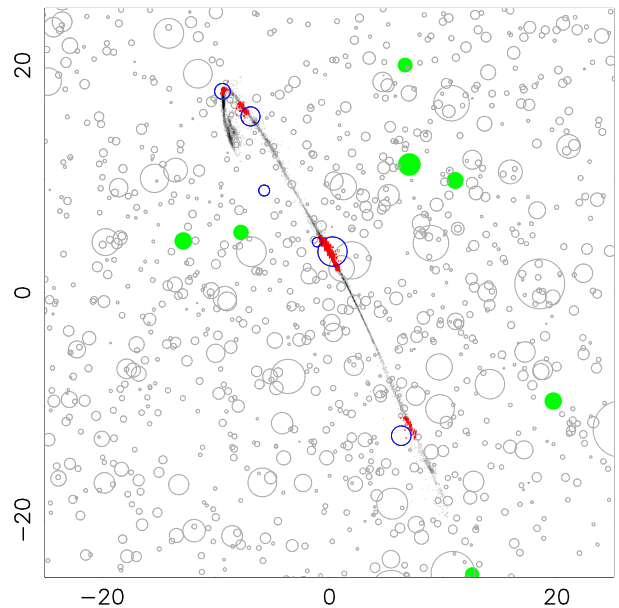


Figure 9. The XY projection one Gyr before the final time of the stream (in greyscale), the dwarf galaxies (filled green circles) and the subhalos (grey circles). Subhalo-stream encounters are shown for subhalos within 2 scale radii of stream particles are blue circles and the particles within 2 scale radii are in red. The distances are in kpc.

cal simulation. Consequently the detailed stream model presented here is a lower bound on the effects of subhalos on the C-19 stream.

The C-19 stream track is defined as passing through the approximate mean of the stars in the $\phi_1 = [-10, 10]$ region in Yuan et al. (2022). Specifically the progenitor orbit passes through RA=355.0, Dec=25.0 degrees, with a radial velocity of -195 km s^{-1} , proper motion of 1.25 and -2.8 milli-arcsec per year in RAcos(Dec) and Dec at a heliocentric distance of 20 kpc. The progenitor is then integrated in the potential of the MW plus LMC model. No optimization of the stream track coordinates or potential model was undertaken. The resulting orbit is adequately close to the current data for the purposes of this paper. The stream simulations placed the current epoch progenitor position at -10 degrees along the stream track, then integrated the progenitor backward including the full subhalo distribution to the desired start time. The model star cluster was then put at that position and integrated forward to create the model stream. A consequence is that the model leaves the dissolved progenitor in the $\phi_1 = [-40, -10]$ region of the stream. The precise final time progenitor location depends on the details of encounters with subhalos, so varies from run to run.

The C-19 model starts the star cluster at a time of 3 Gyr after the Big Bang. Starting the model star cluster at later times means that there are less subhalos to heat the stream and less time for subhalos to encounter the stream, leading to insufficient heating. The model does a reasonable job of accumulating the subhalo interactions of the central region of the stream, but stream ends are more coherent here than they would be in a full cosmological simulation, as seen in Figure 6.

The subhalos in the mass decade around $10^7 M_\odot$ dominate the perturbations to the stream (Carlberg & Agler 2023; Carlberg et al. 2024). Subhalo stream encounters are sufficiently infrequent that there are significant differences of detail in the stream morphology depending on the detailed stream collision history, hence the phases of the orbits of the subhalos. Therefore a set of simulations is done with the subhalo distribution rotated 30 degrees from 0 to 330 degrees between simulations. The 4 streams that are significantly bifurcated around $\phi_1 = 0$ in the CDM subhalo distribution are not included in Figure 10 because they lead to artificially wide stream widths which the currently measured C-19 sky distribution does not support. The widths of the model streams, calculated as a standard deviation, are shown in the lower panel of Figure 10. At 20 kpc distance 0.5 degrees corresponds to 170 pc or a FWHM of 410 pc. The narrowing of the streams along their length is an effect of orbital motion.

The C-19 model streams have considerable structure along their length, but the structure in these model

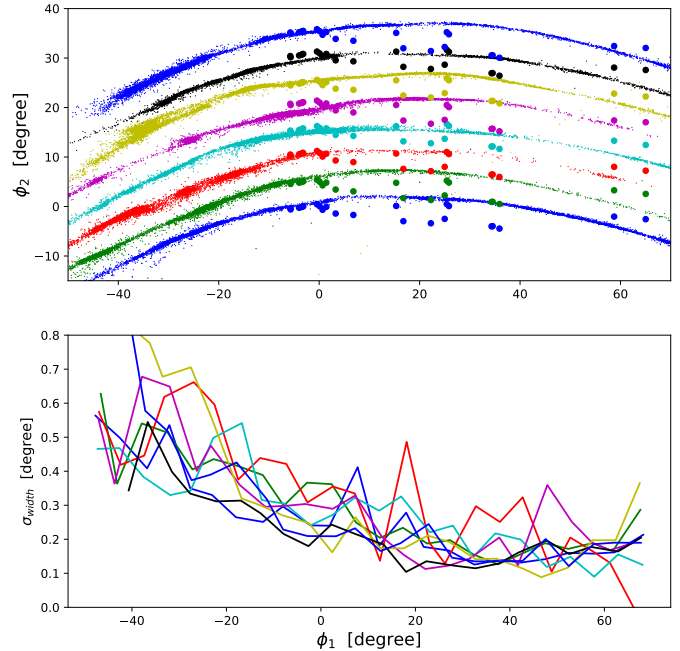


Figure 10. The model streams in C-19 stream coordinates (top) and the standard deviation of their spread about the mean position along the stream (bottom). The subhalo distribution is rotated in steps of 30 degrees from 0 to 330 degrees for a dozen variants of the C-19 model stream. The plot does not show the streams which are bifurcated in the region around $\phi_1 = 0$.

streams is significantly less than the two streams drawn from the full cosmological simulation shown in Figure 6. The movies of the two example streams [CDM Low Mass Clusters](#) show that large scale merging disperses the “ends” of the streams until the main halo settles down around 7 Gyr. The primary halo is not subject to major mergers (by design) for the last 7 Gyr of the simulation so at late times is fairly well represented with the halo potential model used here. At the C-19 start time of 3 Gyr the dominant halo of the full cosmological simulation is about 50% less massive, which mainly effects the orbit, not the subhalo density. The C-19 model potential does not capture the larger scale potential fluctuations due to accretion and merger buildup between 3 and 7 Gyr, but does include the subhalo effects. Therefore the C-19 model is a lower bound on the heating effects.

The line of sight velocities and their dispersion along the streams in the CDM subhalo distribution are shown in Figure 11. The velocity dispersion of C-19, 6.2 km s^{-1} , and its 1-sigma errors from Yuan et al. (2022) is shown in black. The quadrature summed mean of the model streams over $\phi_1 = [-10, 10]$ is $4.1 \pm 1.1 \text{ km s}^{-1}$. The mean velocity dispersion (excluding the bifurcated

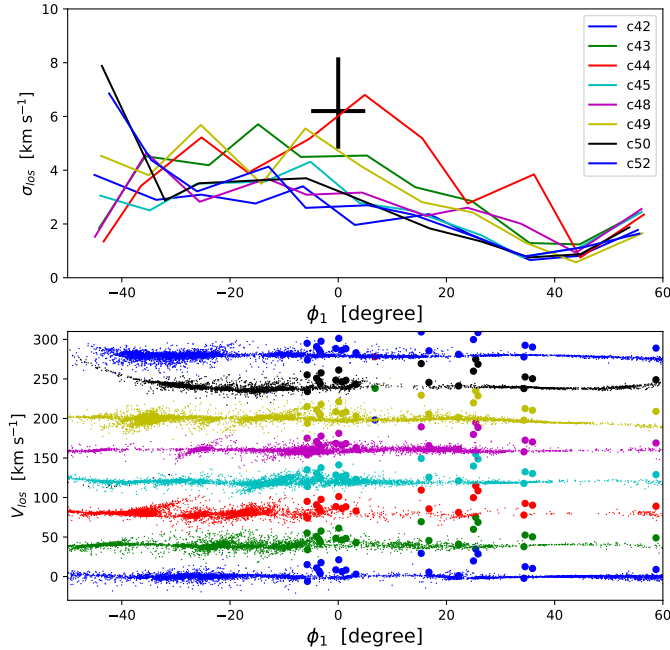


Figure 11. The line of sight velocity dispersion (top) and its distribution along the streams (bottom) for the CDM models of the C-19 stream. The four bifurcated streams are not plotted. The dots show the velocities of the observed C-19 stars. The observational estimate of the velocity dispersion and its one-sigma errors is shown in black.

streams) is within 1.2 sigma (combined) of the observed value. The same modeling procedure for a WDM (5.5 keV) model halo gives velocities shown in Figure 12. Its mean line of sight velocity dispersion of 3.1 ± 0.09 km s^{-1} , a 2.2 sigma difference from the observed value. The small increase in velocity dispersion in the WDM (5.5 keV) model is consistent with the cosmological simulation results (Carlberg et al. 2024). These simulations disfavor the WDM(5.5 keV) model. However given the significant scatter seen in the full cosmological simulation for clusters in the same orbital range, Figure 5, the result is not very strong and emphasizes that stronger conclusions require more than a single stream.

A model stream with no subhalos and no dwarf galaxies (designated c84) is shown in Figure 12. It has a velocity dispersion of 3.6 km s^{-1} in the $\phi_1 = [-10, 10]$ region. Including the known dwarf galaxies (c85) also gives a line of sight velocity dispersion of 3.6 km s^{-1} . The streams velocity dispersion calculated with 3σ clipping are 1.41 and 1.75 km s^{-1} , respectively, indicating unusually strong wings in the velocity profile. The numbers of particles in this section of the two streams are about 20% of those in the models with subhalos which

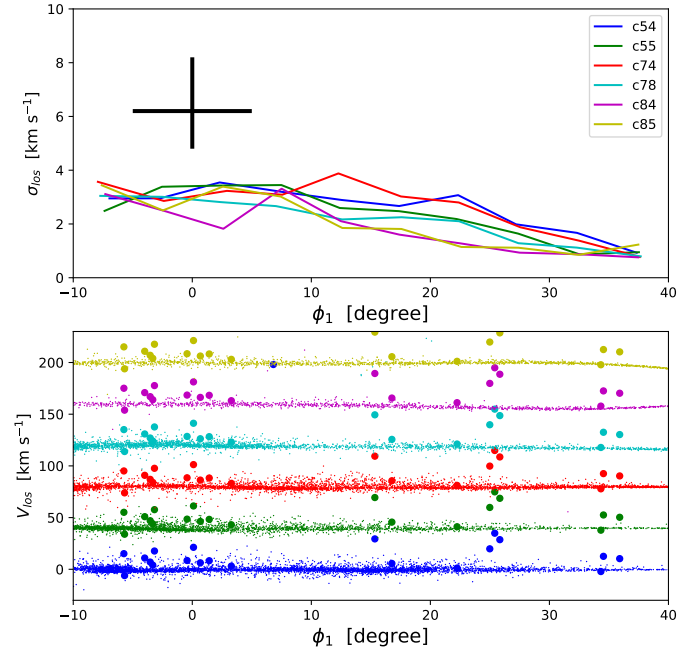


Figure 12. The line of sight velocity distribution for the WDM (5.5 keV) models of the C-19 stream. The top two lines of points are for models with no subhalos and with no dwarf galaxies (purple, second line) and with known dwarf galaxies (yellow, top line). Streams that bifurcate over the plotted stream latitude range are not included.

is a consequence of the subhalo perturbations gradually changing stream orbital phases.

4. DISCUSSION AND CONCLUSIONS

Errani et al. (2022) established, and we confirm, that the dissolution of a globular cluster in a smooth galactic halo cannot explain the the width and line of sight velocity dispersion of the C-19 stream. There are two generic solutions: either the C-19 stream was created from a stellar system hotter and larger than a globular cluster (Errani et al. 2022), or, the velocity dispersion of the stream was increased over the course of its orbital history. We have shown that an old, dissolved, globular cluster stream near apocenter in a galactic halo containing subhalos can explain the kinematics of the C-19 stream, under certain conditions. Detailed modeling of C-19 using a simplified model potential and the subhalos drawn from the cosmological simulations finds that heating C-19 requires the numbers of subhalos found in a CDM cosmology acting on the stream for $\simeq 11$ Gyr. The model finds that the numbers of WDM (5.5 keV) subhalos are insufficient. The subhalo heating of the stream leads to significant density and velocity variations along the stream, Figures 10 and 11, whereas a disrupted dwarf is smooth (Errani et al. 2022). The

currently known numbers of stars do not allow a reliable density profile measurement.

More generally, cosmological Milky Way-like simulations find that dissolved globular cluster streams that are hot and wide near apocenter, like C-19, become thin and cool streams as they orbit through pericenter. The streams discussed here are from progenitor globular clusters with masses below $2 \times 10^4 M_\odot$ and half mass radii in the 3-5 pc range, which have dissolution times in the galactic tidal field of 1-2 Gyr so few stars are added to the streams in the last 5 Gyr.

The width of C-19 as a globular cluster stream is not unique. Streams wider than 0.2 kpc containing globular clusters are listed in Table 1 drawing from the Mateu (2023) compendium (see also Bonaca & Price-Whelan (2024)). There are a total of 27 streams wider than 0.2 kpc, with 5 containing globular clusters and the C-19 stream. The widths are all from Ibata et al. (2021) and therefore use a uniform measurement approach. C-19 may be part of an ancient, extremely metal poor group of streams (Malhan et al. 2022). The wide stream of the distant cluster NGC5466 is excluded because it is likely associated with a merger remnant (Malhan et al. 2022) with a complex orbital history. NGC288 is a complex wide stream (Grillmair 2024). All the listed globular clusters are near the apocenters of their orbits (Baumgardt et al. 2019). These clusters orbit within a few kpc of the bulge, whereas C-19 is less eccentric and has a $\simeq 8$ kpc pericenter. Most of the 22 other wide streams have the abundance spread of a dissolved dwarf galaxy. There should of course be other wide streams from dissolved globular clusters at orbital apocenter but their distance and spread in position and velocity make them harder to find. The distribution of stream widths with current distance in the simulations is shown in Figure 13. About half of the simulated streams are within 30 kpc, whereas about 90% of the Galstreams compendium (Mateu 2023) is within 30 kpc. The radial distribution of streams will have some dependence on the radii at which globular clusters form within pre-galactic subhalos, although that dependence is fairly weak for globular cluster formation within a dwarf galaxy (Carlberg & Keating 2022). On the average the streams are physically wider with galactocentric distance, but approximately the same angular width, around 0.2 degrees.

The hot, wide streams at apocenter become thin, cool streams at pericenter as a result of stream orbital dynamics. Stars are unbound from their progenitor cluster at pericenter in a narrow range of radii, joining the stream with a spread in velocities. The subhalo perturbations to the stream velocities are more likely to occur near orbital pericenter where the subhalo density

Table 1. Wide Globular Cluster Streams

Name	σ_w	r_{GC}	r_{apo}	ecc
	kpc	kpc	kpc	
OmegaCen-I21	0.222	6.5	7.0	0.68
M92-I21	0.231	9.9	10.5	0.83
C-19-I21	0.239	22.9	23.7	0.45
NGC288-I21	0.249	12.9	13.0	0.59
NGC1851-I21	0.546	16.7	19.1	0.92
NGC1261-I21	1.042	18.3	19.3	0.87

is highest. The velocity differences lead to differences in pericenter angle, orbital tilt, and angular momentum which causes the stream particles to spread apart near apocenter. The streams wider than a σ_w of 100 pc in a CDM simulation are on the average about a factor of two hotter than in a WDM (5.5 keV), $7.8 \pm 1.0 \text{ km s}^{-1}$ as compared to $4.1 \pm 1.6 \text{ km s}^{-1}$.

The hot, wide C-19 and thin, cool, GD-1 (Grillmair & Dionatos 2006) streams cover similar radial ranges in their orbits, with the difference in their widths being at least partially explained with C-19 being near apocenter and GD-1 near pericenter. The C-19 model required that it be orbiting in the subhalos of the galaxy for 11 Gyr, which is consistent with the age that being extremely metal poor implies. That is, for C-19 there is very little room for stream age-subhalo abundance degeneracy. GD-1 is less metal poor which opens up the possibility of more age-abundance degeneracy in the stream properties. Finding a common model that explains the internal kinematics of a set of streams is a goal as the data improves.

There is nearly a factor of two velocity dispersion difference between CDM and WDM(5.5 keV) wide streams in the inner halo. The cosmology dependence of long, thin streams, which are generally near pericenter, is present in the wings of the velocity distribution (Carlberg et al. 2024) with a relatively insensitive core Gaussian velocity spread. On the other hand, the cosmology dependence of wide streams, which are generally near apocenter, is in the velocity dispersion itself, which is easier to measure than the core-wing structure of pericenter streams.

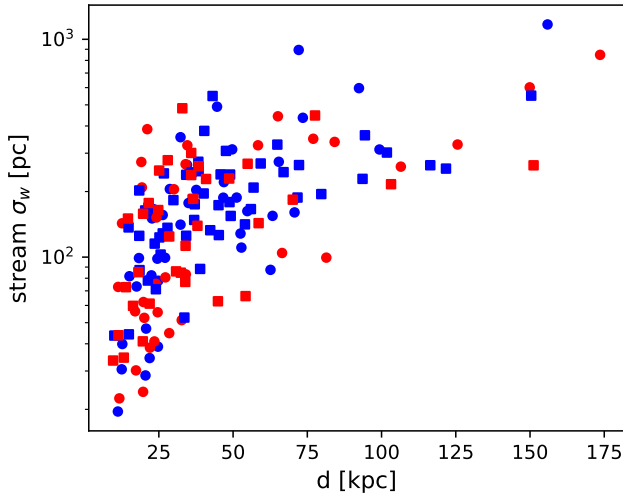


Figure 13. Stream widths with distance. Dissolved clusters are circles, remnant clusters squares, blue CDM, red WDM. Most of the known globular cluster streams are within 30 kpc.

Adrian Jenkins, Carlos Frenk and Andrew Cooper provided invaluable advice and support for computing. This work used the DiRAC@Durham facility managed by the Institute for Computational Cosmology on behalf of the STFC DiRAC HPC Facility (www.dirac.ac.uk). The equipment was funded by BEIS capital funding via STFC capital grants ST/K00042X/1, ST/P002293/1, ST/R002371/1 and ST/S002502/1, Durham University and STFC operations grant ST/R000832/1. DiRAC is part of the National e-Infrastructure. This work used high-performance computing facilities operated by the Center for Informatics and Computation in Astronomy (CICA) at National Tsing Hua University. This equipment was funded by the Ministry of Education of Taiwan, the National Science and Technology Council of Taiwan, and National Tsing Hua University. Computations were performed on the niagara supercomputer at the SciNet HPC Consortium. SciNet is funded by: the Canada Foundation for Innovation; the Government of Ontario; Ontario Research Fund - Research Excellence; and the University of Toronto. CSF acknowledges support by the European Research Council (ERC) through Advanced Investigator grant, DMIDAS (GA 786910). ARJ and CSF acknowledge support from STFC Consolidated Grant ST/X001075/1. APC acknowledges the support of the Taiwan Ministry of Education Yushan Fellowship and Taiwan National Science and Technology Council grant 112-2112-M-007-017-MY3.

Software: Gadget4: [Springel et al. \(2021\)](#), Amiga Halo Finder: ([Gill et al. 2004](#); [Knollmann & Knebe 2009](#)), ROCKSTAR: ([Behroozi et al. 2013](#)), NumPy: ([Harris et al. 2020](#)).

Data Availability: Final snapshots, movies, images, and example scripts are at [CDM Low Mass Clusters](#)

REFERENCES

- Baumgardt, H., Hilker, M., Sollima, A., & Bellini, A. 2019, MNRAS, 482, 5138, doi: [10.1093/mnras/sty2997](https://doi.org/10.1093/mnras/sty2997)
- Behroozi, P. S., Wechsler, R. H., & Wu, H.-Y. 2013, ApJ, 762, 109, doi: [10.1088/0004-637X/762/2/109](https://doi.org/10.1088/0004-637X/762/2/109)
- Binney, J. 1977, MNRAS, 181, 735, doi: [10.1093/mnras/181.4.735](https://doi.org/10.1093/mnras/181.4.735)
- Binney, J., & Tremaine, S. 2008, Galactic Dynamics: Second Edition (Princeton University Press)
- Bonaca, A., Hogg, D. W., Price-Whelan, A. M., & Conroy, C. 2019, ApJ, 880, 38, doi: [10.3847/1538-4357/ab2873](https://doi.org/10.3847/1538-4357/ab2873)
- Bonaca, A., & Price-Whelan, A. M. 2024, arXiv e-prints, arXiv:2405.19410, doi: [10.48550/arXiv.2405.19410](https://doi.org/10.48550/arXiv.2405.19410)
- Carlberg, R. G. 2015, ApJ, 800, 133, doi: [10.1088/0004-637X/800/2/133](https://doi.org/10.1088/0004-637X/800/2/133)
- . 2018, ApJ, 861, 69, doi: [10.3847/1538-4357/aac88a](https://doi.org/10.3847/1538-4357/aac88a)
- Carlberg, R. G., & Agler, H. 2023, ApJ, 953, 99, doi: [10.3847/1538-4357/ace4be](https://doi.org/10.3847/1538-4357/ace4be)
- Carlberg, R. G., Jenkins, A., Frenk, C. S., & Cooper, A. P. 2024, arXiv e-prints, arXiv:2405.18522, doi: [10.48550/arXiv.2405.18522](https://doi.org/10.48550/arXiv.2405.18522)
- Carlberg, R. G., & Keating, L. C. 2022, ApJ, 924, 77, doi: [10.3847/1538-4357/ac347e](https://doi.org/10.3847/1538-4357/ac347e)
- Errani, R., Navarro, J. F., Ibata, R., & Peñarrubia, J. 2022, MNRAS, 511, 6001, doi: [10.1093/mnras/stac476](https://doi.org/10.1093/mnras/stac476)
- Fukushige, T., & Heggie, D. C. 2000, MNRAS, 318, 753, doi: [10.1046/j.1365-8711.2000.03811.x](https://doi.org/10.1046/j.1365-8711.2000.03811.x)
- Gaia Collaboration, Prusti, T., de Bruijne, J. H. J., et al. 2016, A&A, 595, A1, doi: [10.1051/0004-6361/201629272](https://doi.org/10.1051/0004-6361/201629272)

- Garavito-Camargo, N., Besla, G., Laporte, C. F. P., et al. 2019, *ApJ*, 884, 51, doi: [10.3847/1538-4357/ab32eb](https://doi.org/10.3847/1538-4357/ab32eb)
- Gill, S. P. D., Knebe, A., & Gibson, B. K. 2004, *MNRAS*, 351, 399, doi: [10.1111/j.1365-2966.2004.07786.x](https://doi.org/10.1111/j.1365-2966.2004.07786.x)
- Gnedin, O. Y., & Ostriker, J. P. 1997, *ApJ*, 474, 223, doi: [10.1086/303441](https://doi.org/10.1086/303441)
- Grillmair, C. J. 2024, arXiv e-prints, arXiv:2409.17361, doi: [10.48550/arXiv.2409.17361](https://doi.org/10.48550/arXiv.2409.17361)
- Grillmair, C. J., & Dionatos, O. 2006, *ApJL*, 643, L17, doi: [10.1086/505111](https://doi.org/10.1086/505111)
- Harris, C. R., Millman, K. J., van der Walt, S. J., et al. 2020, *Nature*, 585, 357, doi: [10.1038/s41586-020-2649-2](https://doi.org/10.1038/s41586-020-2649-2)
- Helmi, A., & White, S. D. M. 1999, *MNRAS*, 307, 495, doi: [10.1046/j.1365-8711.1999.02616.x](https://doi.org/10.1046/j.1365-8711.1999.02616.x)
- Hernquist, L. 1990, *ApJ*, 356, 359, doi: [10.1086/168845](https://doi.org/10.1086/168845)
- Ibata, R., Malhan, K., Martin, N., et al. 2021, *ApJ*, 914, 123, doi: [10.3847/1538-4357/abfcc2](https://doi.org/10.3847/1538-4357/abfcc2)
- Ibata, R., Malhan, K., Tenachi, W., et al. 2024, *ApJ*, 967, 89, doi: [10.3847/1538-4357/ad382d](https://doi.org/10.3847/1538-4357/ad382d)
- Knollmann, S. R., & Knebe, A. 2009, *ApJS*, 182, 608, doi: [10.1088/0067-0049/182/2/608](https://doi.org/10.1088/0067-0049/182/2/608)
- Malhan, K., & Ibata, R. A. 2018, *MNRAS*, 477, 4063, doi: [10.1093/mnras/sty912](https://doi.org/10.1093/mnras/sty912)
- Malhan, K., Ibata, R. A., Carlberg, R. G., Valluri, M., & Freese, K. 2019, *ApJ*, 881, 106, doi: [10.3847/1538-4357/ab2e07](https://doi.org/10.3847/1538-4357/ab2e07)
- Malhan, K., Ibata, R. A., Sharma, S., et al. 2022, *ApJ*, 926, 107, doi: [10.3847/1538-4357/ac4d2a](https://doi.org/10.3847/1538-4357/ac4d2a)
- Martin, N. F., Venn, K. A., Aguado, D. S., et al. 2022, *Nature*, 601, 45, doi: [10.1038/s41586-021-04162-2](https://doi.org/10.1038/s41586-021-04162-2)
- Mateu, C. 2023, *MNRAS*, 520, 5225, doi: [10.1093/mnras/stad321](https://doi.org/10.1093/mnras/stad321)
- McConnachie, A. W. 2012, *AJ*, 144, 4, doi: [10.1088/0004-6256/144/1/4](https://doi.org/10.1088/0004-6256/144/1/4)
- Meiron, Y., Webb, J. J., Hong, J., et al. 2021, *MNRAS*, 503, 3000, doi: [10.1093/mnras/stab649](https://doi.org/10.1093/mnras/stab649)
- Miyamoto, M., & Nagai, R. 1975, *PASJ*, 27, 533
- Spitzer, L. 1987, *Dynamical evolution of globular clusters* (Princeton University Press)
- Springel, V., Pakmor, R., Zier, O., & Reinecke, M. 2021, *MNRAS*, 506, 2871, doi: [10.1093/mnras/stab1855](https://doi.org/10.1093/mnras/stab1855)
- Starkeburg, E., Martin, N., Youakim, K., et al. 2017, *MNRAS*, 471, 2587, doi: [10.1093/mnras/stx1068](https://doi.org/10.1093/mnras/stx1068)
- Valluri, M., Fagrelus, P., Kuposov, S. E., et al. 2024, arXiv e-prints, arXiv:2407.06336, doi: [10.48550/arXiv.2407.06336](https://doi.org/10.48550/arXiv.2407.06336)
- Viswanathan, A., Yuan, Z., Ardern-Arentsen, A., et al. 2024, arXiv e-prints, arXiv:2405.13124, doi: [10.48550/arXiv.2405.13124](https://doi.org/10.48550/arXiv.2405.13124)
- Yuan, Z., Martin, N. F., Ibata, R. A., et al. 2022, *MNRAS*, 514, 1664, doi: [10.1093/mnras/stac1399](https://doi.org/10.1093/mnras/stac1399)